Chapter 13

Seismic Force Exerted on Structures

Sigiriya means Singha (lion) giri (mountain) in Sanskrit language. King Kasyapa of Sri Lanka who was afraid of his enemy's attack located his palace at the top of this rock. Water was supplied from big pools which were excavated at the top of the rock as well.

13.1 Analysis on Soil–Structure Interaction

Effects of ground shaking on underground structures such as tunnels and basements are often analyzed by connecting structures with free field of ground (1D soil columns without effects of embedded structures) by means of (nonlinear) springs, see Fig. 13.1a. Springs are classified into those concerning normal earth pressure and those transmitting shear force. This method of analysis is called the method of seismic displacement, the method of subgrade reaction, or the method of Winkler foundation. The modulus of springs has long been studied in the fields of, for example, pile foundation (nonlinear subgrade reaction modulus). The horizontal response (time history of displacement) of a one-dimensional soil column is first calculated by using wave propagation theory in a level ground (Sect. 4.1 and Chap. 8). The calculated motion is then substituted at the support of springs, which generate dynamic response of the structure.

Strictly speaking, the method in Fig. 13.1a is not sufficient. Suppose a soil mass embedded in a free field consisting of the same type of soil. Since no relative displacement occurs between the soil mass and the free field, because of the same material type, spring mechanisms are not activated, causing no motion in the soil mass in the analysis. This problem is solved by superimposing stress components in the free field (Fig. 13.1b). Thus, a strict analysis requires a free-field calculation of both displacement time history and the stress time history, which are then substituted in a soil-structure interaction analysis (Fig. 13.1b). In most practical cases, the magnitude of free-field stress is less significant than the spring forces and the stress superposition is ignored.

(a) Structures connected to free field by springs

(b) Rigorous method of seismic displacement with superimposed free-field stress around the structure.

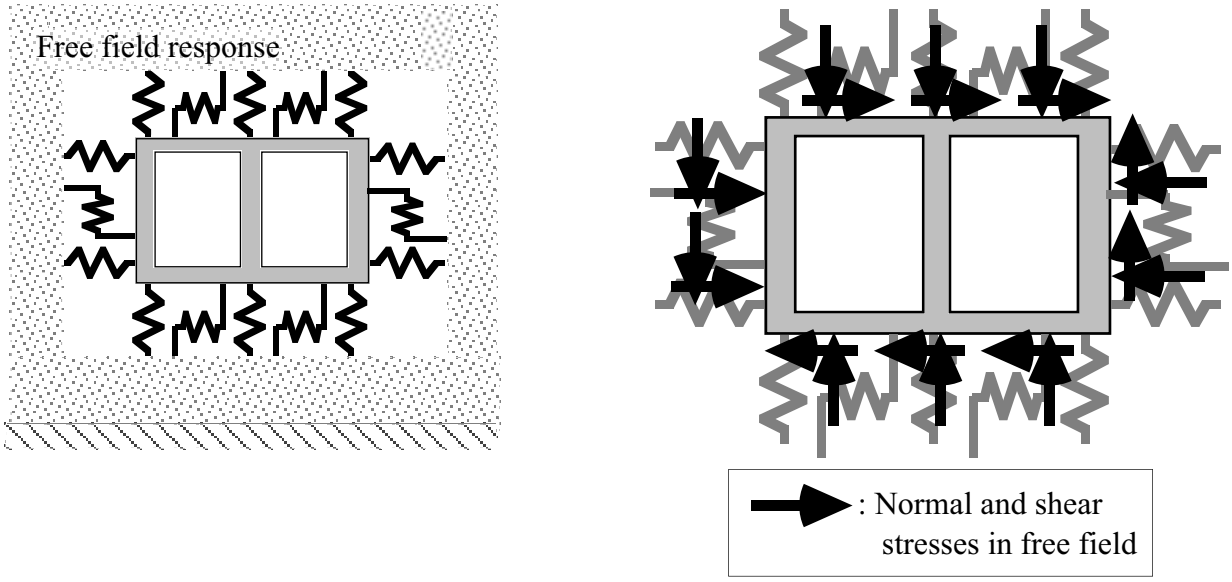

Fig. 13.1 Method of seismic displacement

An example of an elaborate method of analysis is illustrated in Fig. 13.2 in which a dynamic finite element analysis was conducted on nonlinear soil models and elastic model of a Daikai subway station in Kobe which collapsed during the 1995 Kobe earthquake. Conventionally, it had been believed that tunnel was safe during earthquakes because shaking at depth is weaker and the surrounding stiff ground prevents large deformation of tunnels in mountains (Sect. 13.7). Such an idea did not hold true when shaking was extremely strong and the surrounding soil was not very stiff; Daikai station was constructed in an excavated pit and then backfilled.

One of the limitations of the dynamic analysis in Fig. 13.2 was that the complicated nonlinear behavior of the structural members (columns and slabs) was not taken into account. This was because the employed computer code could not handle nonlinear deformation characteristics of both soil and concrete at the same time. To overcome this problem, the maximum calculated forces exerted by surrounding soil elements upon the structural elements were applied statically on the nonlinear model of the subway station (Fig. 13.3). Nonlinear springs at connection of columns and slabs stand for the nonlinearity of the structure. This analysis was able to reproduce the failure of central columns (Fig. 13.4), which consequently caused the significant subsidence at the ground surface (Fig. 13.5). This lesson triggered reinforcement of central columns in many other subway stations. See examples in Tokyo (Figs. 13.6 and 13.7).

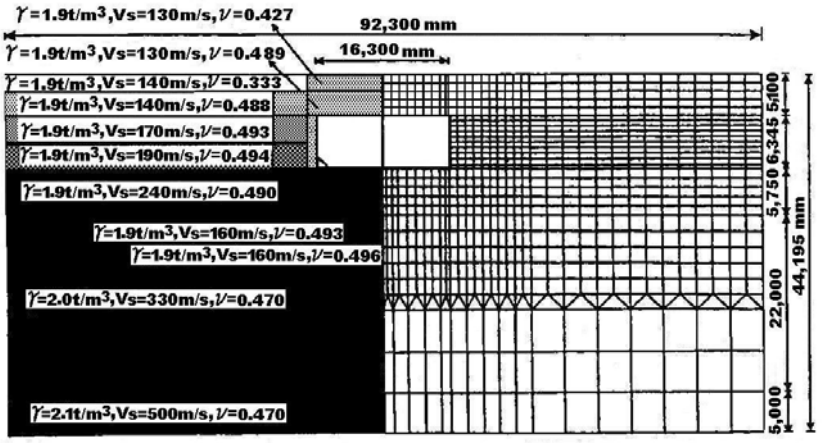

Fig. 13.2 FE model of failed subway station (Nakamura et al., 1996)

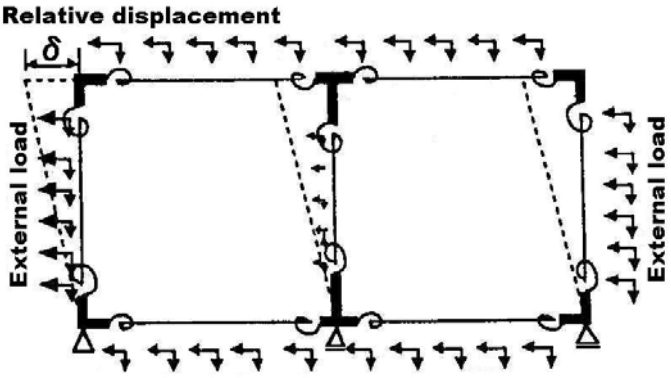

Fig. 13.3 Static nonlinear analysis of subway station. (Nakamura et al., 1996)

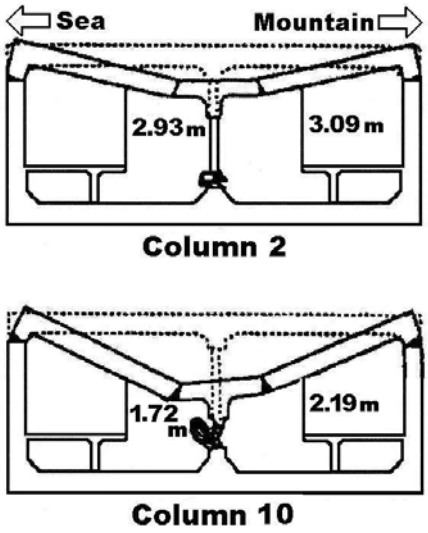

Fig. 13.4 Collapse of columns at the center of station (Nakamura et al., 1996)

Theoretically the dynamic soil–structure interaction is often decomposed into the inertial and kinetic interaction; Fig. 13.8 illustrates an example of a structure supported by a single pile. The inertial interaction means the force which is the mass of the super structure × its acceleration and is exerted on the foundation. The kinetic interaction is the force that is caused by the differential displacement between soil and the foundation. Springs in Fig. 13.1 stand for the kinetic interaction. Both kinds of force induce dynamic deformation and possibly failure.

Fig. 13.5 Ground subsidence above Daikai subway station (by Nozomu Yoshida)

Fig. 13.6 Reinforced central columns in Kasuga Station of Tokyo Metropolitan Subway

Fig. 13.7 Reinforced central columns in Daimon Station of Tokyo Metropolitan Subway

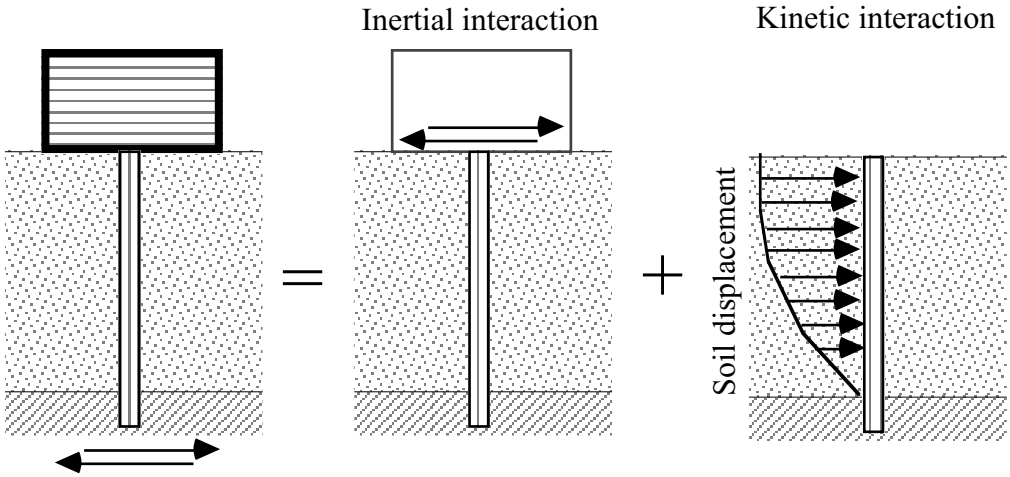

Fig. 13.8 Schematic illustration of dynamic soil–structure interaction

13.2 Seismic Design of Embedded Pipeline

Embedded pipelines for gas, water, electricity, and communications are subjected to earthquake effects such as buckling, bending failure, and separation at joints. Since these seismic effects are caused by distortion of ground, the seismic design of embedded pipelines puts emphasis on soil–structure interaction; the seismic inertia force is therein less important.

Figure 13.9 illustrates the concept of seismic design in which the ground consists of two layers, a soft surface deposit and a stiff engineering base. In this figure a pipeline is connected with the surface soil by springs (elastic beam resting on Winkler foundation). This figure concerns only with bending of a pipe because the springs are perpendicular to the axis of the pipe. Figure 13.10 illustrates another application of the method to lateral response of a pile. The use of (linear or nonlinear) springs between an embedded structure and free ground motion is called the method of seismic displacement and is widely practiced in design of piles as well.

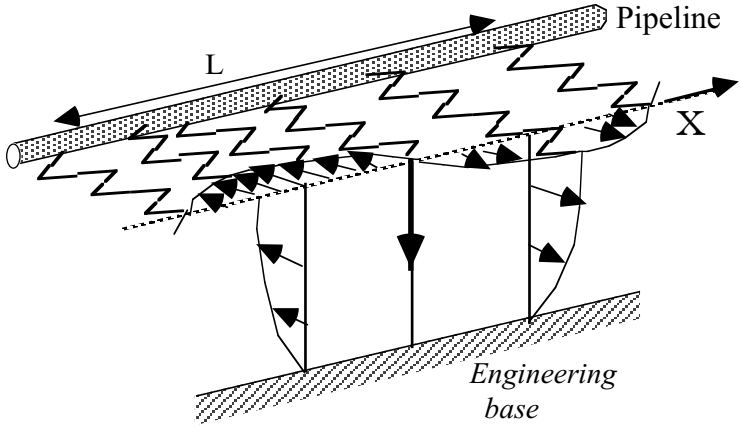

Fig. 13.9 Analysis on soil–pipeline interaction

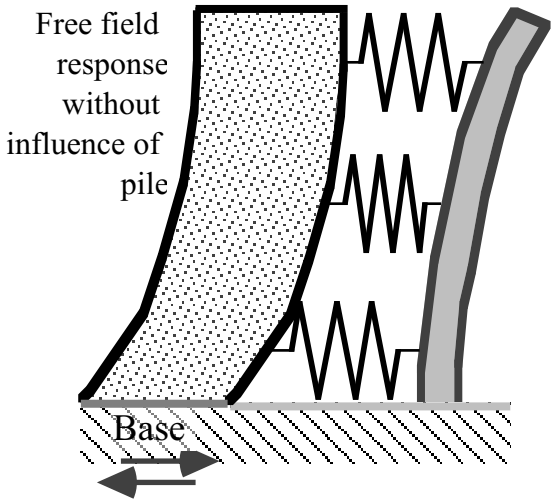

Fig. 13.10 Method of seismic displacement as applied to lateral response of pile

The seismic input is given by the amplitude of soil displacement, u, which is idealized by

$$u(z) = U \cos\frac{\pi z}{2H}\sin\frac{2\pi x}{L} \qquad (13.1)$$

where z is the depth below surface, U is the surface displacement amplitude, and L is the wave length of surface displacement. The displacement varies in a harmonic manner in both x and z directions. This ground displacement exerts lateral forces on the pipeline through spring connections. Since the magnitudes of ground displacement and spring forces vary in the x direction, the pipeline is subjected to bending.

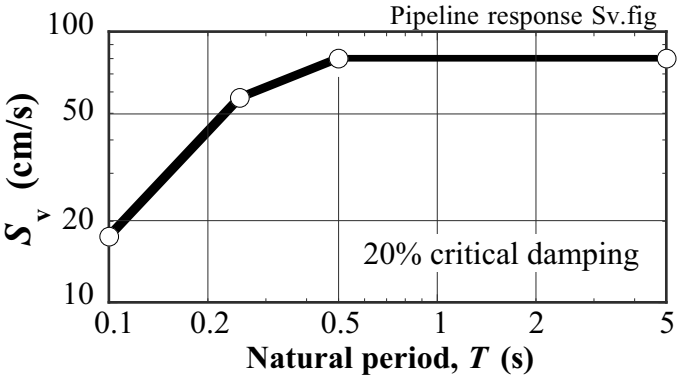

Fig. 13.11 Example of design velocity response spectrum

The surface displacement, U, in (13.1) is given for design purposes by the following procedure.

1. The seismic coefficient (Sect. 7.1) in the engineering base is specified as K_H.
2. The (relative) velocity response spectrum (Sect. 23.1) of a design earthquake motion in the base is normalized by the seismic coefficient and is designated by S_v. Hence, $K_H S_v$ is the design velocity response of the surface soil, which is idealized by a single-degree-of-freedom model as the theory of response spectrum states. See Fig. 13.11 for example of S_v, while K_H is 0.65 for example. Note in this figure that the response spectrum, S_v, is a function of natural period, T.
3. The natural period of the surface deposit, T, is calculated by $T = 4H/V_s$ where V_s is the S-wave velocity of soil (6.30). It is assumed that the surface shaking occurs in a harmonic manner under this natural period.
4. Since the amplitude of velocity in the surface soil is $K_H S_v(T)$, the displacement amplitude is given by

$$\begin{aligned}&\text{Displacement amplitude} = \text{ Velocity amplitude/ Circular frequency}\\ &= \left[K_H S_v(T)\right]/(2\pi/T).\end{aligned} \tag{13.2}$$

5. Since the displacement, U, at the surface of a soil column is $4/\pi$ times greater than that of a single-degree-of-freedom model, (13.1) is modified to be

$$u(z) = \frac{4}{\pi} \times \frac{T}{2\pi} K_H S_v(T) \cos\frac{\pi z}{2H} \sin\frac{2\pi x}{L} = \frac{2T}{\pi^2} K_H S_v(T) \cos\frac{\pi z}{2H} \sin\frac{2\pi x}{L}. \tag{13.3}$$

   For derivation of $4/\pi$ parameter, refer to Sect. 13.3.
6. The wave length, L, for design is determined in practice as the harmonic mean of two wave lengths

$$L = 2L_1L_2/(L_1 + L_2), \tag{13.4}$$

where $L_1 = V_s T = 4H$, V_s the S-wave length in the surface soil, and $L_2 = (V_s$ in the engineering base$) \times T$.

13.3 Amplification: Soil Column Vs. Spring–Mass Model

A comparison is going to be made of seismic amplifications of a realistic soil column and its equivalent single-degree-of-freedom model, see Fig. 13.12. The properties of the soil column are uniform while the single-degree-of-freedom model consists of a lumped mass and an elastic spring. They are called equivalent when their natural periods are identical. The response of these two models to the base acceleration of $A \sin \omega t$ is going to be studied.

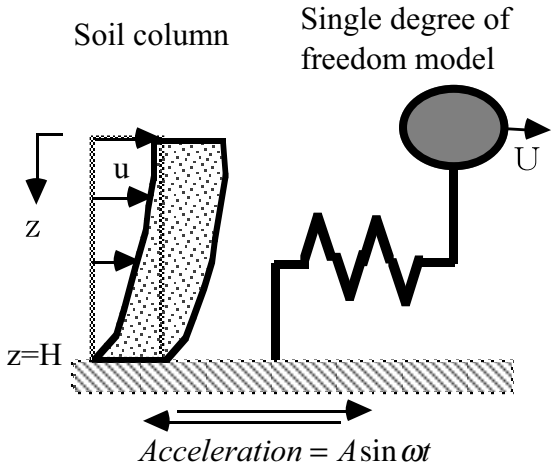

Fig. 13.12 Soil column and spring–mass model

The response of the lumped mass model is governed by

$$\frac{\mathrm{d}^2 U}{\mathrm{d}t^2} + \omega_{\mathrm{o}}{}^2 U = -A \sin \omega t, \tag{13.5}$$

where U is the displacement relative to the base, $\mathrm{d}^2U/\mathrm{d}t^2$ its second time derivative, and ω_{o} the natural circular frequency of the model.

Similar to the discussion on lifeline earthquake engineering (Fig. 13.9), the displacement of a soil column, u, is approximated by the fundamental harmonic mode of response

$$u(z,t) = U(t) \cos \frac{\pi z}{2H}, \tag{13.6}$$

in which *U(t)* is the unknown time history of surface displacement. The governing equation of motion for *U(t)* in (13.6) is derived by using the theory of Lagrangean equation of motion (Sect .25.3). First, the kinetic energy of the soil column, K, is expressed in terms of U

$$K = \frac{\rho}{2} \int_0^H \left(\frac{\mathrm{d}u}{\mathrm{d}t} \right)^2 \mathrm{d}z = \frac{\rho}{2} \int_0^H \cos^2 \frac{\pi z}{2H} \mathrm{d}z \times \left(\frac{\mathrm{d}U}{\mathrm{d}t} \right)^2 = \frac{\rho H}{4} \left(\frac{\mathrm{d}U}{\mathrm{d}t} \right)^2. \tag{13.7}$$

The potential energy due to strain of the soil column is denoted by Q

$$Q = \frac{G}{2} \int_0^H \left(\frac{\mathrm{d}u}{\mathrm{d}z} \right)^2 \mathrm{d}z = \frac{G}{2} \int_0^H \left\{ \frac{\mathrm{d}}{\mathrm{d}z} \left(\cos \frac{\pi z}{2H} \right) \right\}^2 \mathrm{d}z \times U^2 = \frac{GH}{4} \left(\frac{\pi}{2H} \right)^2 U^2. \tag{13.8}$$

The potential energy due to the inertia force is denoted by I

$$I = \rho \int_0^H U \cos \frac{\pi z}{2H} A \sin \omega t \, \mathrm{d}z = \rho A \frac{2H}{\pi} \sin \omega t \times U. \tag{13.9}$$

Equations (13.6)–(13.8) are substituted in the Lagrangean equation of motion

$$\frac{\mathrm{d}}{\mathrm{d}t} \left\{ \frac{\partial (K - Q - I)}{\partial (\mathrm{d}U/\mathrm{d}t)} \right\} - \frac{\partial (K - Q - I)}{\partial U} = 0. \tag{13.10}$$

Consequently,

$$\frac{\rho H}{2}\frac{\mathrm{d}^2U}{\mathrm{d}t^2}+\frac{GH}{2}\left(\frac{\pi}{2H}\right)^2U=-\rho A\frac{2H}{\pi}\sin\omega t \quad \text{or} \quad \frac{\mathrm{d}^2U}{\mathrm{d}t^2}+\frac{G}{\rho}\left(\frac{\pi}{2H}\right)^2U=-A\frac{4}{\pi}\sin\omega t. \tag{13.11}$$

Accordingly, the natural circular frequency of the soil column is given by

$$\omega_o=\frac{2\pi}{\text{Natural period}}=\frac{2\pi}{4H/V_\mathrm{s}}=\frac{\pi}{2H}\sqrt{\frac{G}{\rho}}. \tag{13.12}$$

Equation (13.11) is simplified to be

$$\frac{\mathrm{d}^2U}{\mathrm{d}t^2}+\omega_\mathrm{o}{}^2U=-\frac{4}{\pi}\times A\ \sin\omega t \tag{13.13}$$

By comparing (13.5) and (13.13), which are of a similar appearance, it is found that the surface motion of a soil column (13.13) is $4/\pi$ times greater than the response of a spring-mass model when their natural periods are made identical. This finding was used in derivation of (13.3). The factor of $4/\pi$ is called the participation factor (刺激係数).

13.4 Rigorous Compaction of Soil Column and Equivalent Spring–Mass Model

The assumption of harmonic variation of displacement along a soil column (z direction) is removed from the discussion in the preceding Sect. 13.3. The harmonic response of a spring-mass model is obtained by solving

$$\frac{\mathrm{d}^2U}{\mathrm{d}t^2} + \omega_o{}^2 U = -A\ \sin\omega t. \qquad (13.14)$$

Hence,

$$U = \frac{A}{\omega^2 - \omega_{\mathrm{o}}{}^2}\sin\omega t = \frac{A}{\omega^2}\frac{1}{1-\left(\omega_{\mathrm{o}}/\omega\right)^2}\sin\omega t. \qquad (13.15)$$

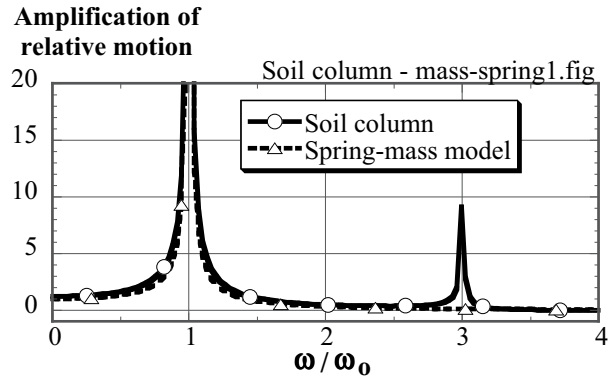

Fig. 13.13 Amplification of relative displacement in uniform soil column and equivalent mass-spring model

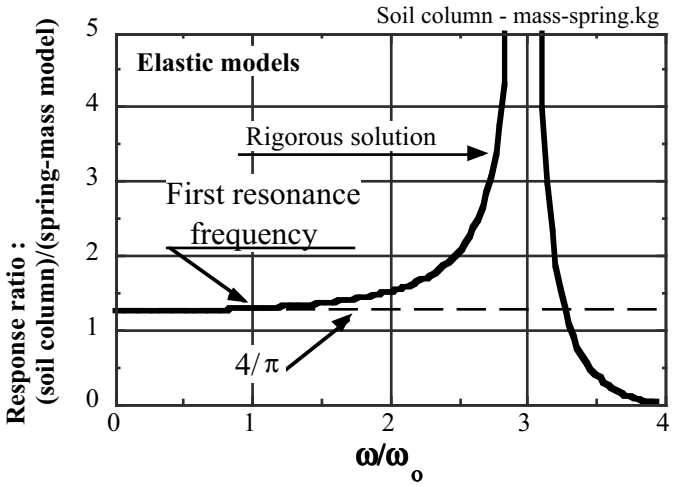

Fig. 13.14 Comparison of response of soil column and equivalent spring-mass model

The response of a uniform soil column is obtained by considering the wave propagation. By paying attention to the fact that the concerned displacement, $u(z,t)$, is a relative displacement to the base displacement of $-A\ \sin\omega t/\omega^2$,

$$u(z,t) = \frac{A}{\omega^2}\left\{1 - \frac{\cos\dfrac{\omega z}{V_{\mathrm{s}}}}{\cos\dfrac{\omega H}{V_{\mathrm{s}}}}\right\}\sin\omega t. \qquad (13.16)$$

At the ground surface, $z = 0$, in particular,

$$u(z=0,t) = \frac{A}{\omega^2}\left\{1 - \frac{1}{\cos\dfrac{\omega H}{V_{\mathrm{s}}}}\right\}\sin\omega t = \frac{A}{\omega^2}\left\{1 - \frac{1}{\cos\left(\dfrac{\pi}{2}\dfrac{\omega}{\omega_{\mathrm{o}}}\right)}\right\}\sin\omega t, \qquad (13.17)$$

in which $\omega_{\mathrm{o}} = \left(\pi V_{\mathrm{s}}\right)/2H$ was taken into account. Note again that this $u(z=0,t)$ is the surface displacement relative to the base.

The behaviors of a soil column and its equivalent spring-mass model are compared by using a common value of ω_o. Figure 13.13 illustrates that the amplification curves of two models look similar except that the spring-mass model does not have the second resonance peak due certainly to its single degree of freedom. The ratio of the amplification, however, reveals that two models are different:

$$\text{Ratio of amplitude} = \frac{\text{Amplitude at surface of soil column}}{\text{Amplitude of spring} - \text{mass model}}.$$

$$= \left\{1 - \left(\frac{\omega_o}{\omega}\right)^2\right\}\left[1 - \frac{1}{\cos\left\{\frac{\pi}{2}\left(\frac{\omega}{\omega_o}\right)\right\}}\right] \tag{13.18}$$

Figure 13.14 compares (13.18) against the simplified solution of $4/\pi$ that was derived in Sect. 13.3. It is found therein that the approximate solution is acceptable in the lower frequency range; being valid at least up to the first resonance frequency.

13.5 Seismic Water Pressure on Wall

Dam engineering has been interested in the water pressure exerted by a reservoir (貯水池, 水庫) subjected to a seismic inertia force. Westergaard (1931) developed a theory that can calculate this dynamic pressure by assuming a semi-infinite reservoir water facing a vertical quay wall (Fig. 13.5). The total water pressure acting on a wall is given by

Water pressure = Hydrostatic pressure + Westergaard pressure

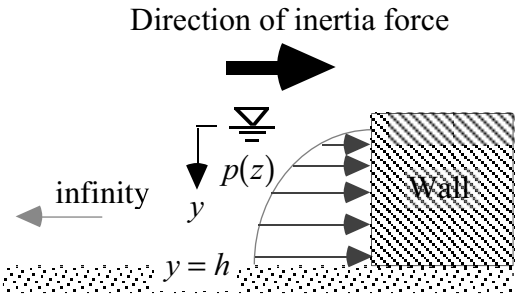

Fig. 13.15 Westergaard´s dynamic reservoir pressure

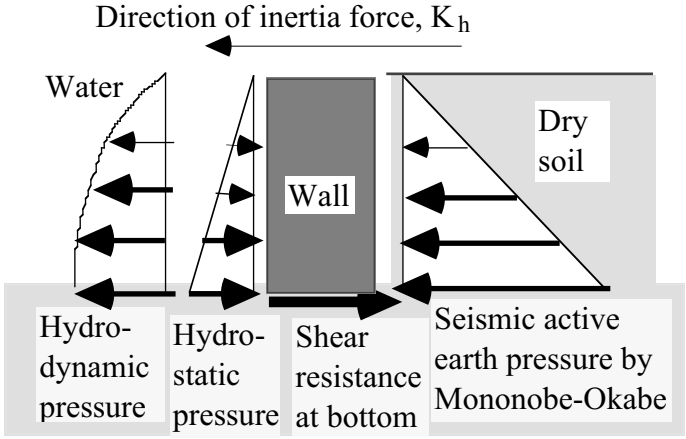

Fig. 13.16 Forces acting on water-front wall of gravity type

Westergaard derived a series solution (級数解) of the dynamic water pressure. The distribution of this pressure was reasonably approximated by a parabola (see Fig. 13.15),

$$p = \frac{7}{8} K_{\mathrm{h}} \gamma_{\mathrm{w}} \sqrt{hy}\,, \qquad (13.19)$$

where p is the hydrodynamic pressure at a water depth of y, K_{h} the horizontal seismic coefficient, γ_{w}, the unit weight of water, and h the depth of reservoir. By integrating (13.19) from $y = 0$ to $y = h$,

$$\text{Total hydrodynamic force} = \frac{7}{12} K_{\mathrm{h}} \gamma_{\mathrm{w}} h^2. \qquad (13.20)$$

The point of action of the Westergaard pressure is found as

$$y = \frac{\int_0^h \frac{7}{8} K_{\mathrm{h}} \gamma_{\mathrm{w}} \sqrt{hy} \times y \, \mathrm{d}y}{\frac{7}{12} K_{\mathrm{h}} \gamma_{\mathrm{w}} h^2} = \frac{3}{5} h\,, \qquad (13.21)$$

while the hydrostatic pressure has a triangular distribution and acts at 1/3 from the bottom.

Figure 13.16 illustrates the lateral forces acting on a revetment wall at a water front. Note that the hydrodynamic pressure decreases the water pressure because the inertial force is oriented towards the reservoir water. Accordingly, the lateral stability of the wall is lost when

(Seismic active earth pressure calculated by Mononobe–Okabe theory)
– (Hydrostatic water pressure) + (Westergaard hydrodynamic pressure)
– (Shear resistance at the bottom)

is positive. Note further that the direction of the hydrodynamic pressure is identical with the direction of the inertia force, consequently decreasing the total water pressure. The above calculation does not care the moment equilibrium that concerns the rotation of the wall.

The backfill soil in Fig. 13.16 is dry and unrealistic for simplicity. When this soil is water-saturated, (1) accumulation of excess pore water pressure due to dilatancy, and (2) dynamic fluctuation (動的変動) of pore water pressure due to inertia force have to be taken into account. The accumulation of excess pore water pressure will be discussed after Sect. 17.1 concerning liquefaction. Section 24.17 will address the application of Westergaard theory to dynamic earth pressure in liquefied subsoil.

Matsuo and O-Hara (1965) developed a theory on the amplitude of pore pressure fluctuation in pervious soil. This amplitude is about 70% of the Westergaard pressure, oriented in the direction of K_{h}. They reported their shaking table tests to show a good agreement between prediction and observation.

13.6 Dynamic Earth Pressure Exerted by Water Saturated Backfill

In most design practice, the seismic earth pressure exerted by water-saturated back fill is calculated by simply modifying the Mononobe–Okabe active earth pressure formula (Sects. 12.5 and 12.7);

$$P_{\mathrm{ae}} = \frac{K_{\mathrm{ae}}}{2}\gamma H^2, \qquad (13.22)$$

in which the seismic earth pressure coefficient, K_{ae}, changes with the seismic coefficient, K_{h}, in terms of the angle, ψ (Fig. 13.17).

The Mononobe–Okabe formula consists of two mechanisms. The one is a mechanism of shear resistance. Since shear strength is governed by the effective stress, the unit weight as employed in the earth pressure formula has to be the buoyant unit weight, $\gamma' = \gamma - \gamma_{\mathrm{w}}$. The problem is that the mass of existing pore water is removed from the analysis.

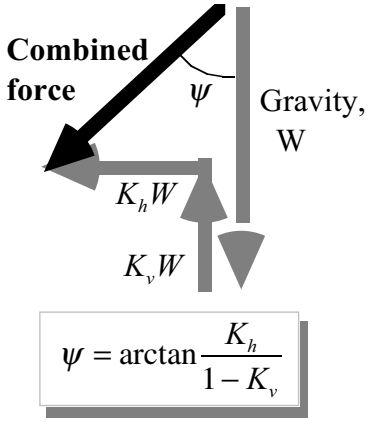

Fig. 13.17 Definition of orientation of combined force

Fig. 13.18 Active seismic failure of quay wall and tilting of building behind the wall

The use of γ' in place of γ in (13.22) is not sufficient. This is because the seismic force is exerted on mass of both soil grains and pore water. Unless the permeability of soil is extremely high, soil grains and pore water move together. Thus, the inertia force is given by $K_{\mathrm{h}}\gamma$ and $K_{\mathrm{v}}\gamma$; note that γ is used here and not γ'. Therefore, the calculation of seismic earth pressure should employ both γ for inertia force and γ' for shear resistance. Equation (13.17), however, can make use of only one kind of unit weight.

In practice, (13.22) should use γ',

$$P_{\mathrm{ae}} = \frac{K_{\mathrm{ae}}}{2}\gamma' H^2. \qquad (13.23)$$

However, the seismic coefficient in the horizontal direction has to be modified in order to take into account the horizontal inertia force. Therefore, the seismic coefficient, K'_{h}, is defined by

$$K'_{\mathrm{h}} \equiv \frac{\gamma}{\gamma'} K_{\mathrm{h}}. \qquad (13.24)$$

Accordingly,

$$\psi' = \arctan\frac{K'_{\mathrm{h}}}{1-K_{\mathrm{v}}} = \arctan\left(\frac{K_{\mathrm{h}}}{1-K_{\mathrm{v}}}\frac{\gamma}{\gamma'}\right) \tag{13.25}$$

The new seismic earth pressure coefficient, K_{ae}, is calculated by using (13.25). For an example of seismic active earth pressure exerted by water-saturated backfill, see Fig. 13.18. This wall moved towards the sea and the backfill moved together. Consequently, a pile foundation of a building on the left side was destroyed and the building tilted towards the sea.

13.7 Damage in Tunnels Caused by Earthquakes

It has been conventionally believed that tunnels have good resistance against shaking, most probably. The first reason for this is that the intensity of shaking in rock under the ground is weaker than the surface acceleration (Fig. 13.14). The second reason is because the rock mass around a tunnel has sufficient rigidity to keep the shape of the tunnel unchanged. Even when tunnels are intersected with causative faults, no fatal collapse occurred (Sect. 16.7). This traditional idea is not always correct, however, as illustrated by the following examples. Remarks on subway tunnels were made in Sect. 13.1.

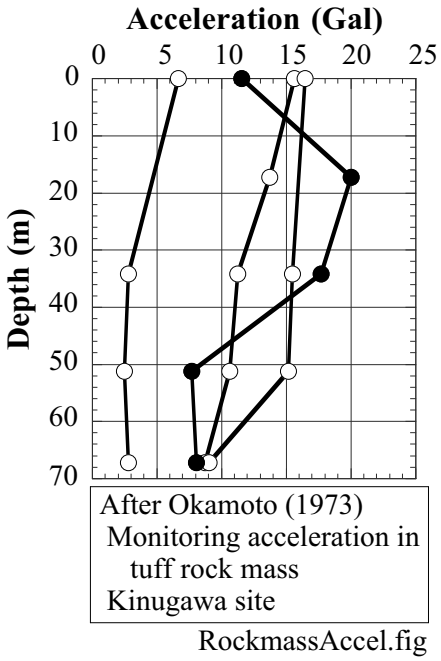

Fig. 13.19 Acceleration recorded in rock mass

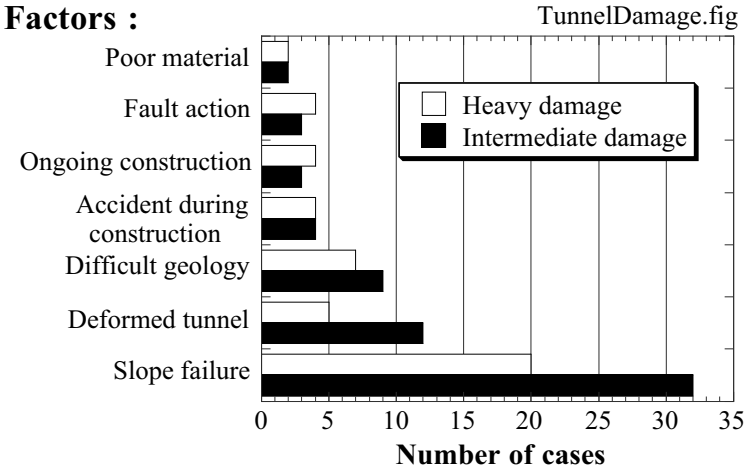

Fig. 13.20 Factors concerning seismic damage of tunnels (JRTT, 1996)

Fig. 13.21 Collapsed Kinoura tunnel during the 1992 Noto-Hanto-Oki earthquake

Figure 13.20 is a summary of earthquake-induced problems in tunnels. The number of events related with seven situations are illustrated therein. It is noteworthy that the majority of problems were caused by slope instability at the entrance. The second majority is related with difficult geology and deformation that had been going on prior to earthquakes. In contrast, the number of cases is small concerning poor tunnel materials such as deterioration, fault action, ongoing construction, and tunnels that experienced collapse or other accident during construction.

Fig. 13.22 Mountain behind entrance of Kinoura tunnel

Fig. 13.23 Slope failure at the entrance of tunnel (五龍隧道 Taiwan, 1999)

Figure 13.21 illustrates collapse of a tunnel during the 1992 Noto-Hanto-Oki earthquake (能登半島沖地震). This Kinoura (木の浦) tunnel had a overburden soil of only 22 m (Fig. 13.22), which collapsed into the tunnel. It was possible at the time of inspection to see the sun light through the collapsed tunnel from inside the tunnel. One of the common problems caused by earthquakes in tunnels is the slope failure near the entrance (Fig. 13.23). Slope reinforcement or construction of a protective structure is thus important. Another source of problem lies in a fault (Sect. 16.7).

The dynamic shaking and ground pressure may affect tunnels. Figure 13.24 indicates the significant distortion of Haguro Tunnel during the 2004 Niigata-Chuetsu earthquake. While the weak bottom of the tunnel (road pavement) buckled due to lateral compression, the top part developed longitudinal cracks due to superposition of bending and compression (Fig. 13.25). The distortion of Haguro Tunnel is related to the following two issues. First, the rock around the tunnel is young and soft as evidenced by a large landslide that occurred immediately next to the tunnel entrance (Fig. 13.26). The shortage in rigidity made it difficult for the tunnel to maintain its shape. Second, the bottom part of the tunnel (invert) did not develop arching action and was not very rigid, thus being vulnerable to compression and buckling failure. The compression in the bottom easily resulted in extension in the top (Fig. 13.27). Since the Haguro Tunnel was very important in a local road network, it was restored within six months by replacing the damaged concrete by new one. Note that a similar damage and collapse were experienced in a subway tunnel in Kobe (Sect. 13.1).

Tunnel damages due to fault action will be discussed in Sect. 16.7.

Fig. 13.24 Distorted shape and buckling of pavement in Haguro Tunnel, Niigata-Chuetsu

Fig. 13.25 Tension crack in top part of Haguro Tunnel

Fig. 13.26 Landslide near the western entrance of Haguro Tunnel

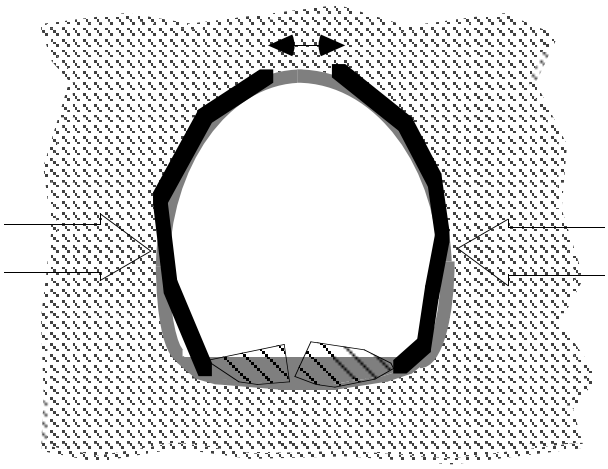

Fig. 13.27 Schematic illustration of deformation mechanism of Haguro Tunnel

13.8 Nodular Pile

Pile foundation is often damaged by strong earthquake motion. One reason for the damage is the inertial action due to mass of a super structure, and the other is the kinematic action induced by shaking ground. Figure 13.28 illustrates an example of pile damage due to inertial effects.

Past experiences showed good performance of a type of pile, which is called a nodular pile. Being a prefabricated prestressed concrete pile, a nodular pile has an irregular shape and develops increased skin friction. Figure 13.29 indicates a nodular-pile foundation in Kobe Port Island after the quake in 1995, Although it was located immediately behind a damaged quay wall, the foundation was able to survive the significant soil displacement. Moreover, Fig. 17.39 shows a building that was supported by nodular piles and survived the subsoil liquefaction. More precisely, the columns and roofs that were supported by nodular piles had no damage, while the concrete block floors suffered significant distortion because they simply rested on ground and were not connected to the stable structural members.

Fig. 13.28 Damaged pile in Navrakhi Harbor, Gujarat Province, India, in 2001

Fig. 13.29 Nodular pile foundation in Kobe Rokko Island in 1995 (Japan Pile Inc., 2007)

A nodular pile is an embedded pile whose installation process is illustrated in Fig. 13.30. First, a hole is bored by an auger (Fig. 13.30a), and then the auger moves back and forth in the hole, while jetting grout and mixing it with soil (Fig. 13.30b). After sufficient mixing, a nodular pile is pushed downwards from the surface (Fig. 13.30c). After curing time, the pile and the surrounding cement-mixed soil forms a body of pile. Since the injected grout has high w/c ratio (water/cement being typically 100%), the pile has much higher rigidity than the soil.

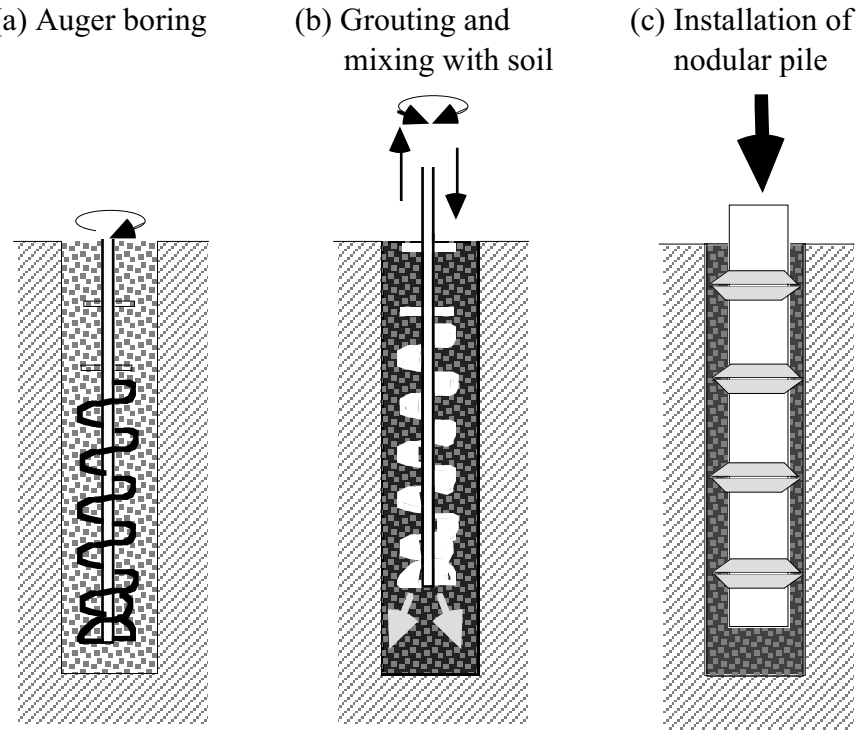

Fig. 13.30 Installation of nodular pile

Figure 13.31 shows nodular piles prior to installation. The diameter of the main shaft is 300 mm or more and the minimum diameter of nodes is 440 mm. The spacing between nodes is 1 m. It is possible to connect two or more piles for deeper installation. Figure 13.32 indicates two stages during pile installation; auger boring and pushing of a pile.

Fig. 13.31 Nodular piles prior to installation

Fig. 13.32 Installation of nodular pile

In the current design practice, the increased bearing capacity of a nodular pile is attributed to the pile diameter, which is increased by the enlarged nodules and the surrounding cement-mixed soil. In reality, the bearing capacity is increased by the force transfer from the pile axis to the surrounding soil by means of nodules (Yabuuchi, 2007). It seems that the compressed soil under a node expands laterally, increases the horizontal effective stress along the pile shaft, and further increases the skin friction, see Fig. 13.33.

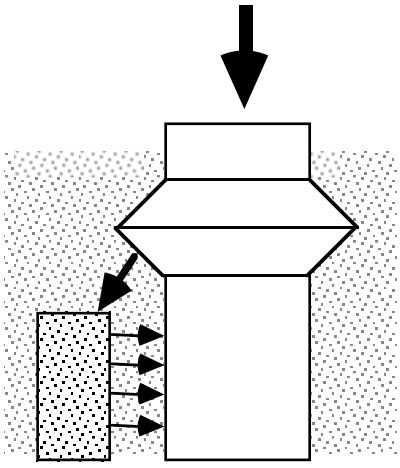

Fig. 13.33 Probable mechanism of increased skin friction of nodular pile

Fig. 13.34 Soil container for model tests on vertical bearing capacity of nodular pile

Fig. 13.35 Model of nodular pile for bearing capacity tests

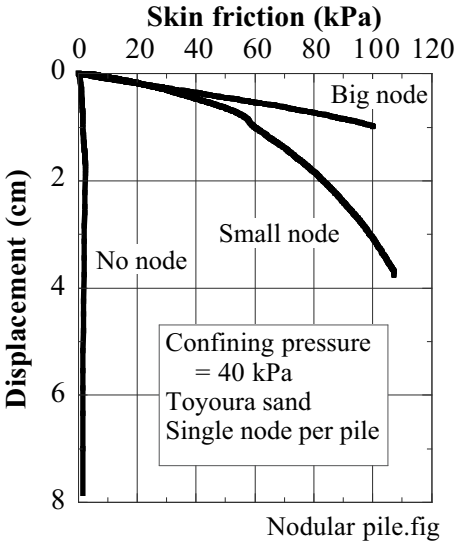

Fig. 13.36 Displacement vs. skin friction curves for model piles with and without node

To further study this issue, model tests were conducted (Borda et al., 2007) in a container (Fig. 13.34) that has air bags at the ground surface so that overburden pressure would be applied for better reproduction of in-situ stress conditions. Figure 13.35 reveals an employed model pile that measures 4.0 cm in diameter and is of one or a few simplified node. The diameter of the node measured either 6.4 cm (small node) or 7.1 cm (big node). The measured relationship between skin friction and vertical displacement of a pile is presented in Fig. 13.36 for the case of single node. It is therein seen that a plain pile without node achieved the ultimate but negligible skin friction after a small displacement and this friction was maintained constant under larger displacement. In contrast when a node was attached to a pile, the skin friction increased gradually with displacement and finally the magnitude of friction was remarkably greater than that of a plain pile. Note, however, that the behavior of a nodular pile undergoing lateral load is yet to be known.

List of References in Chapter 13

Borda, O., Uno, M. and Towhata, I. (2007) Shaft capacity of nodular piles in loose sand, Proc. 49th Nat. Conf. Japan. Geotech. Soc., Vol. 2, pp. 1175-1176.

Japan Pile Corporation (2007) Behavior of nodular piles during 1995 Kobe earthquake, Internal Report (in Japanese).

JRTT (Japan Railway Construction, Transport, and Technology Agency) (1996) Guideline for Design and Construction of NATM Tunnels, p. 49 (in Japanese).

Matsuo, H. and O-Hara, S. (1965) Dynamic pore water pressure acting on quay walls during earthquakes, Proc. 3rd World Conf. Earthq. Eng., Vol. 1, pp. 130–141.

Nakamura, S., Yoshida, N. and Iwatate, T. (1996) Damage to Daikai subway station during the 1995 Hyogoken Nanbu earthquake and its investigation, The 1995 Hyogoken-Nanbu Earthquake, JSCE Committee of Earthquake Engineering, pp. 287–295.

Okamoto, S. (1973) Introduction to earthquake engineering, Univ. Tokyo Press, p. 62.

Westergaard, H.M. (1931) Water pressure on dams during earthquakes, Transactions of ASCE, Paper, No. 1835, pp. 418–433.

Yabuuchi, S. (2007) The behavior of nodular piles in sand: calibration research on cylindrical and nodular piles packed with gravel or slag, accepted by Soils Found.